Ultrasonics Sonochemistry 79 (2021) 105780

Contents lists available at ScienceDirect

Ultrasonics Sonochemistry

journal homepage: www.elsevier.com/locate/ultson

Effect of ultrasonic treatment on the activity of sugar metabolism relative enzymes and quality of coconut water

Jilin Wu [a], Haiming Chen [a,b], Wenxue Chen [a], Qiuping Zhong [a], Ming Zhang [a,*], Weijun Chen [a,*]

[a] College of Food Science and Engineering, Hainan University, 58 Renmin Road, Haikou, Hainan 570228, PR China
[b] Maritime Academy, Hainan Vocational University of Science and Technology, 18 Qingshan Road, Haikou, Hainan 571126, PR China

ARTICLE INFO

Keywords:
Coconut water
Ultrasound
Sugar metabolism
Acid invertase
Inactivation

ABSTRACT

In this study, tender coconuts were treated with high-intensity ultrasound (US) for 20 min at a frequency of 20 kHz and a power of 2400 W. Compared with control group, US treated coconut water had a higher content of total soluble solid and sugar/acid ratio along with a lower pH value and conductivity, and the contents of sucrose, fructose and glucose were also higher. Results from HS-SPME/GC–MS showed that there was no significant difference in the content of volatile compounds in coconut water before and after US treatment. The activities of sugar metabolism enzymes such as sucrose phosphate synthase, sucrose synthase, acid invertase (AI) and neutral invertase were inhibited by US, of which AI had the strongest inactivation. Circular dichroism and fluorescence spectra showed that the secondary and tertiary structure of AI molecule were destroyed with the increase of US intensity and time, which was confirmed by the change of particle size distribution pattern and scanning electron microscopy. Molecular docking and molecular dynamics showed that US treatment prevented the recognition and binding of sucrose and AI molecules, thereby inhibiting the decomposition of sucrose. In conclusion, our results indicate that US can inhibit the activity of AI and maintain the sugar content to increase the quality as well as extend the shelflife of coconut water, which will bring more commercial value.

1. Introduction

Tender coconuts (*Cocos nucifera L.*) refer to coconuts that have matured for 6–9 months, whose water can be directly consumed or processed into various beverages. Coconut water is highly valued due to its nutritional characteristics and special flavor. It contains a remarkable content of salts, minerals, vitamins, sugars, amino acids and enzymes [1–3]. Among these compounds, sugars are the main component of soluble solids in coconut water, and the sweetness is an important criterion for evaluating the quality [4]. The main sugars in tender coconut water are glucose, fructose and sucrose, followed by sorbitol, galactose, xylose and mannose. However, the sugar content in coconut water tends to decrease, thus giving rise to serious damage to its quality during storage and processing, which has gained widespread and increasing concern in coconut industry [5].

The decreasing of sugar is mainly relative to various metabolic activities catalyzed by enzymes, especially sugar metabolism enzyme. Sugar metabolism process of coconut water is mainly regulated by four key enzymes [6,7], including sucrose phosphate synthase (SPS), sucrose synthase (SS), acid invertase (AI) and neutral invertase (NI). SPS catalyze fructose-6-phosphate to form sucrose phosphate, which will further generate sucrose under the action of sucrose phosphatase. SS reversibly catalyzes the synthesis of sucrose from free fructose and glucose, including sucrose synthase-synthesis (SS-s) and sucrose synthase-cleavage (SS-c). As invertases, both AI and NI are responsible for irreversibly converting sucrose into glucose and frucrose [8,9].

Various methods have been used to inactivate enzymes during fruit storage and processing, including thermal processing, refrigeration and chemical treatment. Among them, ultrasound (US) technology has gained much attention due to its safety and protection to the original flavor of food [10]. The effect of US is mainly attributed to the cavitation effect caused by the generation, growth and implosion of tiny bubbles [11]. The frequency range of high-power US is between 20 kHz and 100 kHz, which can generate huge shear forces and large amounts of free radicals in liquid medium [12]. These free radicals can react with some key amino acid residues involved in enzyme stability, substrate binding or catalytic function, thus resulting in the loss of enzyme activity [13]. Besides, huge shear forces can disrupt the interactions (such as hydrogen bonds, van der Waals forces, electrostatic interactions, hydrophobic interactions, etc.) that maintain the secondary and tertiary structure of

* Corresponding authors.
E-mail addresses: zhangming-1223@163.com (M. Zhang), chenwj@hainanu.edu.cn (W. Chen).

https://doi.org/10.1016/j.ultsonch.2021.105780
Received 3 August 2021; Received in revised form 14 September 2021; Accepted 1 October 2021
Available online 6 October 2021

protein, resulting in the loss of protein physiological functions and enzyme inactivation [14–16].

In addition, US treatment is often combined with pressure to enhance the efficiency of enzyme inactivation [17]. Pressure can reduce the vapor pressure of the system, thereby improving the efficiency and strength of bubble implosion and free radical generation [18]. Tender coconut is a natural closed system and can create a pressurized environment for US. To the best of our knowledge, the effect of US on the activity of enzymes related to sugar metabolism in coconut water has not been reported so far. Therefore, this study aims to inveistage how high-intensity US regulate the activity of sugar metabolism relative enzymes and affect the quality of coconut water during storage. The quality of coconut water was determined, including physical and chemical properties, volatile components and sugar content. The activity of enzymes relative to sugar metabolism was investigated. Moreover, the mechanism of US on AI inactivation was explored by circular dichroism (CD), fluorescence spectroscopy, particle size distribution (PSD), scanning electron microscopy (SEM), molecular docking and molecular dynamics.

2. Material and methods

2.1. Materials and chemicals

Tender coconuts that are 8 months old and uniform in color, and have no damage or insect-borne infection on the surface, were purchased from a local fruit market in Hainan. AI (I885089, ≥200 U/mg) was purchased from Macklin Biochemical Co. (Shanghai, China). All other reagents used were of analytical grade.

2.2. Sample preparation

Ultrasound group (UG) was treated with US for 20 min at a frequency of 20 kHz and a power of 2400 W by a 3000 W US processor (XC-3000, Jining Xinxin ultrasonic electronic equipment Co., Ltd., Jining, China) at 25 °C and control group (CG) did not get any treatment. All samples were stored in a ventilated place at room temperature. Tender coconuts were opened and sampled at 0, 3, 6, 9, 12 and 15 days of storage. Samples were collected in foil bags, frozen in liquid nitrogen, and immediately placed in a −80 °C refrigerator. In order to eliminate biological differences between samples, 12 tender coconuts were opened at the same time and coconut water was collected, of which 4 tender coconuts were mixed into one sample for a total of 3 parallel samples [2].

2.3. Physical and chemical analysis of coconut water

Total soluble solid (TSS) contents were measured using a PAL-2 portable refractometer (Japan Atago Co., Ltd., Tokyo, Japan), calibrated with distilled water before measurement, and the results were displayed in °Brix [19]. Then, pH value was measured by a FE20 pH meter (Mettler Toledo Co., Ltd., Zurich, Switzerland), and the conductivity was measured by a FE30 conductivity meter (Mettler Toledo Co., Ltd., Zurich, Switzerland). Sugar/acid ratio was defined as °Brix/pH value. All measurements were carried out in triplicate.

2.4. Determination of volatile compounds in coconut water

Five mL of coconut water was placed in a 20 mL headspace vial and added 2 g of sodium chloride. Headspace vial was sealed with a Teflon-lined silica cap and equilibrated at 50 °C for 10 min under constant stirring. Solid phase microextraction (SPME) fiber (DVB/CAR/PDMS, Supelco, Bellefonte, PA, USA) was exposed in headspace vial for 60 min, and then placed in gas chromatography-mass spectrometer (GC/MS) in electron ionization (EI) mode (internal ionization source, 70 eV) with a scan range of m/z 35 to 300 for desorption and measurement. Separation was carried out on a DB-WAX (30 m × 0.25 mm × 0.25 μm) fused silica capillary column. The heating program of column oven is 40 °C for 3 min, 5 °C/min to 120 °C, 10 °C /min to 250 °C, and hold for 5 min. Helium gas was used as carrier gas with a flow rate of 1 mL/min.

2.5. Determination of fructose, glucose and sucrose content

All samples were thawed at 4 °C, then diluted 20 times with ultrapure water, and passed through a 0.45 μm Millipore filter for later use. The content of glucose, fructose and sucrose was determined by a high performance liquid chromatography (HPLC) system (Agilent 1260, Agilent Technologies Inc., USA) equipped with four-stage pump, autosampler, column oven and refractive index detector (RID). 10 μL of sample was injected into HPLC system fitted with a NH_2-RP analytical column (4.6 × 250 mm, 5 μm, Shanghai ANPEL Scientific Instrument Co., Ltd., Shanghai, China). The temperature of autosampler and column oven was set to 4 °C and 35 °C, respectively. Aqueous solution of acetonitrile (acetonitrile: water = 70: 30, v/v) was used as mobile phase, with a flow rate of 1.0 mL/min.

2.6. Determination of enzyme activity related to sugar metabolism

All samples were thawed at 4 °C, and enzyme activity of AI, NI, SPS and SS was determined by enzyme activity detection kit (Beijing Solarbio Science & Technology Co., Ltd., Beijing, China).

2.6.1. Determination of AI and NI activity

In the experimental group, samples and standard sucrose solution were added and incubated in a 37 °C water bath for 30 min, after which the supernatant was centrifuged at 12,000 g and 4 °C for 5 min. The supernatant was added with 3, 5-dinitrosalicylic acid for color development, and the absorbance value was measured at 540 nm. One unit of AI and NI activity was defined as the production of 1 μg reducing sugar per mg of protein per min at 37 °C. All assays were performed three times and corrected with sucrose-deficient blanks. The difference between the measurement methods of AI and NI was the pH value of the buffer (pH value of AI buffer was 4.5, and NI was 7.0).

2.6.2. Determination of SPS and SS activity

The sample was added to the buffer containing uridine diphosphate (UDP)-glucose and incubated in a water bath at 25 °C for 10 min. The synthesized sucrose was reacted with resorcinol and the absorbance difference was determined at 480 nm. One unit of SPS and SS activity was defined as the production of 1 μg sucrose per mg of protein per min at 25 °C. All assays were performed three times and corrected with a blank lacking fructose-6-phosphate. Unlike SPS, fructose was added when measuring sucrose synthase and all assays were corrected with blanks lacking fructose for the SS-s assay and UDP for the SS-c assay.

2.7. Ultrasonic treatment of AI

AI (1 mg/mL) was dissolved in 50 mM disodium hydrogen phosphate-citrate buffer (pH 4.5). The protein solution placed in a mixture of ice and water was treated by US at a frequency of 20 kHz with different time (5 to 30 min, 200 W) and power (100 to 600 W, 20 min) using a 1000 W US processor (JY92-2D, Ningbo Scientz Biotechnology Co., Ltd., Ningbo, China) equipped with a probe tip with a diameter of 0.636 cm for US treatment [20].

2.8. CD spectrum measurement

Chirascan-plus Circular Dichroism Spectrometert (Applied Photophysics Ltd., Leatherhead, Surrey, England) was used to record CD spectra using a quartz cuvette with an optical path of 1 mm at room temperature. CD spectra were scanned in the far ultraviolet range (190–260 nm) with a speed of 50 nm/min. The protein solutions of 0.5 mg/mL were prepared in 50 mM disodium hydrogen phosphate-citrate buffer (pH 4.5). Protein-free buffer was used as the blank, and the

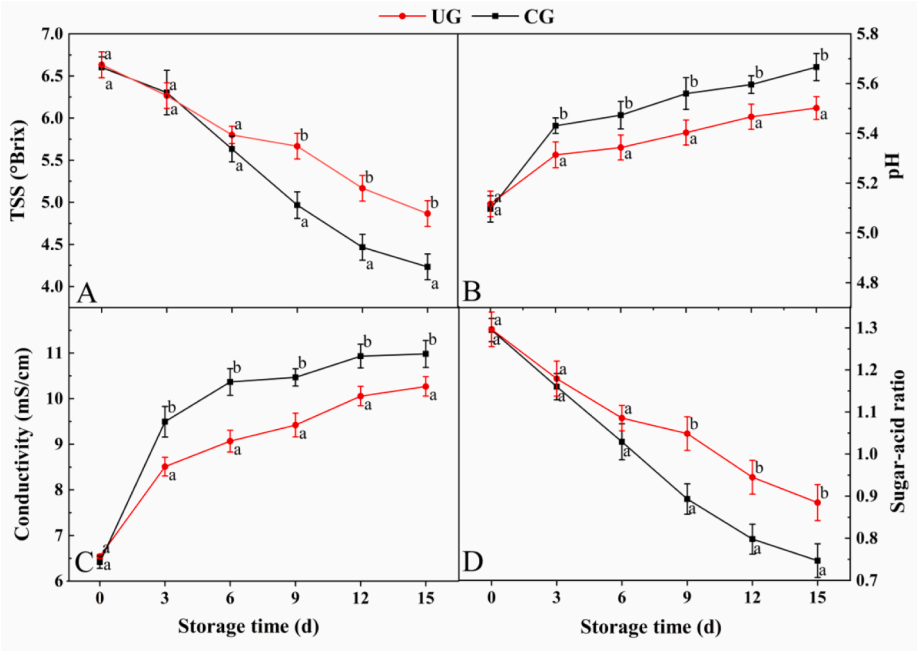

Fig. 1. TSS (A), pH (B), conductivity (C) and sugar/acid radio (D) of coconut water during storage. The data are presented as mean values ± standard deviations (n = 3). Mean values with different letters are significantly different ($p < 0.05$).

sampling time-per-point is 0.5 s. The obtained data were expressed as molar extinction coefficient difference (mdeg), and the content of different secondary structures were calculated by CDNN 2.0 software [21].

2.9. Fluorescence spectrum measurement

Fluorescence spectrum was conducted with a F-280 Spectrophotometer (Gangdong Science & Technology Co., Ltd., Tianjin, China). Samples were scanned in the wavelength range of 300–400 nm with the maximum excitation wavelength (λ_{ex} = 330 nm) at room temperature, and both the excitation and emission slits were 5 nm [22,23].

2.10. PSD measurement

Particle size of native and US-treated AI solved in 50 mM disodium hydrogen phosphate-citrate buffer (pH 4.5) was recorded with Zetasizer Nano ZS90 instrument (Malvern Instruments, Malvern, Worcestershire, UK) at room temperature.

2.11. SEM measurement

The freeze-dried samples were fixed on the sample stage, sprayed with gold, coated with a gold film in a vacuum evaporator, and then placed in a SEM (Verios G4 UC, Thermofisher Scientific Co., Ltd., Massachusetts, USA) to observe the microstructure with an acceleration voltage of 50 kV and a magnification of 5000 times.

2.12. Molecular docking

Autodock Tools were used for molecular docking. The structure of AI was obtained from RCSB Protein Data Bank (PDB ID: 3KF3). The molecular structure of sucrose was obtained from PubChem. The receptor remained rigid, and the ligand remained flexible. The autogrid box parameter was set to 40 Å × 40 Å × 40 Å, and the grid spacing parameter was 0.375 Å. The calculation was performed using the Lamarckian genetic algorithm (LGA), and other parameters were set to default values [24]. Discovery Studio 4.5 Client was used to analyze docking results.

2.13. Molecular dynamics

GROMACS 4.6.5 package was used for molecular dynamics simulation. Protein and small molecule were processed using Amber99SB-ILDN and GAFF force field, respectively. Each system was solvated within a cube box of TIP3P water molecule with a 12 Å distance around the solute. The SHAKE algorithm was used to limit the stretching vibration of all hydrogen bonds, and simulation step was set to 2 fs. Simulation used periodic boundary conditions, and cutoff value of non-bond interaction was set at 0.8 nm. Ewald (PME) method was used for calculating long-range electrostatic effects. The entire system was optimized using 5000-step steepest descent method first, followed by 5000-step conjugate gradient method. After optimization, the system was gradually heated from 0 to 300 K under the canonical (NVT) ensemble, and the heating time is 300 ps. Then each system was balanced for 1 ns under NPT (300 K, 1 atm) conditions. Finally, a 100 ns simulation was performed in NPT ensemble with isothermal and pressure [25,26].

2.14. Statistical analysis

All experimental results were expressed as mean ± standard deviation (SD). The significance of data was performed using one-way analysis of variance (ANOVA), followed by Tukey's multiple comparisons using SPSS version 24.0 statistical software (SPSS Inc., Chicago, Illinois, USA), with a 95% confidence level, meaning that differences were considered as statistically significant when $p < 0.05$.

3. Results and discussion

3.1. Changes in the physical and chemical properties of coconut water

Sugar accounts for 80% of TSS in coconut water, and the main sugars include glucose, fructose and sucrose. As can be seen from Fig. 1A, TSS contents of UG and CG showed a decreasing trend during the entire storage process. From the sixth day, TSS content of UG was significantly higher than that of CG. TSS content of UG at day 15 was 4.9 °Brix, which was significantly higher than that of CG with 4.2 °Brix. During the whole storage process, pH value of UG and CG showed an upward trend, and

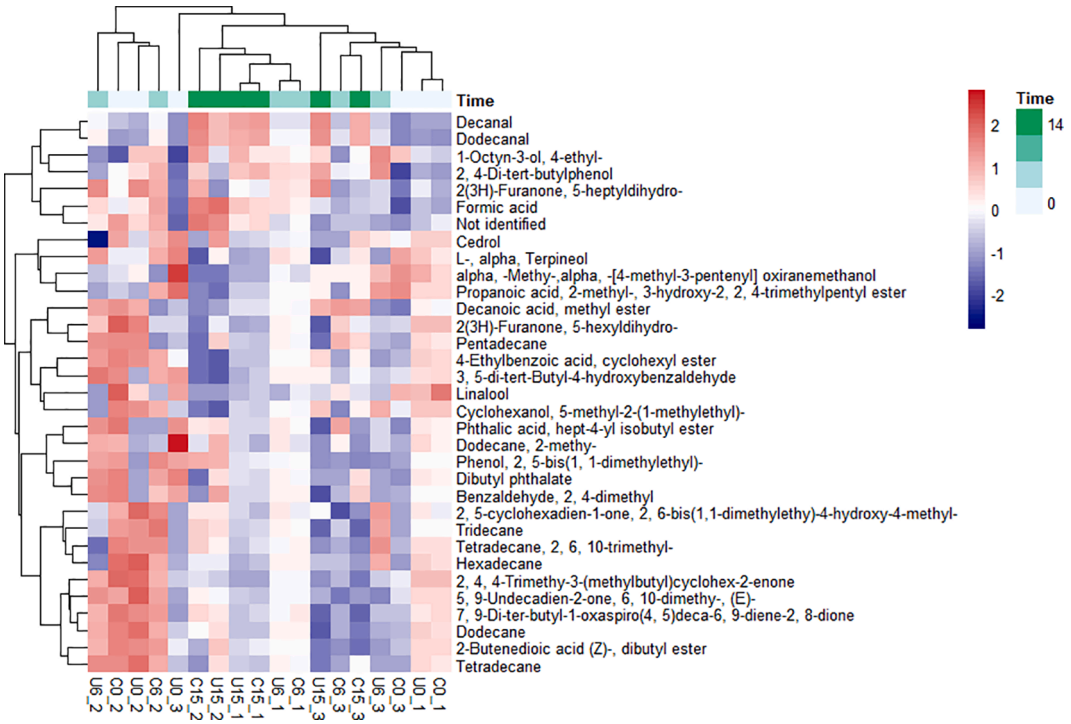

Fig. 2. Heatmap of relative contents of volatile compounds in coconut water at different storage time of UG and CG.

the pH value of UG was lower than that of CG (Fig. 1B). This may be attributed to the fact that tender coconut still maintains high metabolic activities (such as tricarboxylic acid cycle, gluconeogenesis, fermentation and amino acid interconversion) after harvest, in which oxalic acid, tartaric acid, pyruvic acid and malic acid are quickly consumed [27].

With the increase of storage time, conductivity showed an increasing trend, and conductivity of UG increased more moderately than that of CG. The conductivity of both UG and CG increased quickly within the first 3 days, with the value of CG rose from 6.4 mS/cm to 9.5 mS/cm and UG rose from 6.5 mS/cm to 8.5 mS/cm, and then slowly increased from 6 to 15 days (Fig. 1C). This trend reflects the penetration of cytoplasmic electrolyte from coconut kernel during storage, in which the quality of tender coconuts decreases first and then becomes stable [28]. Sugar/acid ratio is an important index affecting the taste, quality and shelf life of coconut water [29]. It can be seen from Fig. 1D that sugar/acid ratio showed a downward trend throughout the storage period and the value of UG was higher than that of CG. Sugar/acid ratio of UG decreased slowly, indicating that the quality of the samples was relatively stable during the storage period.

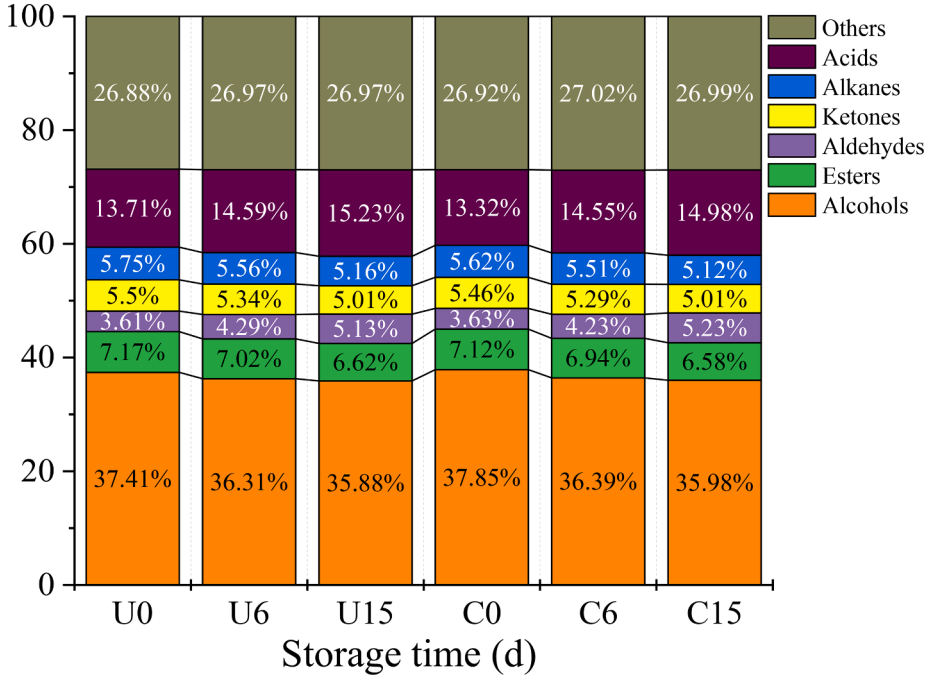

Fig. 3. Relative contents of volatile compounds in coconut water at different storage time of UG and CG.

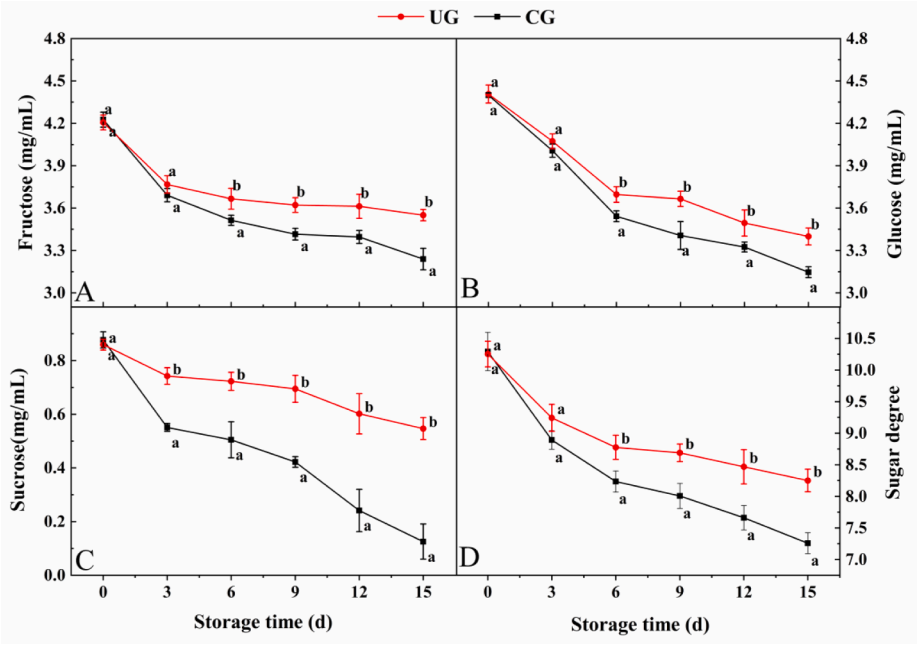

Fig. 4. Effect of US treatment on the content of fructose (A), glucose (B) and sucrose content (C) as well as sugar degree (D) in coconut water stored at room temperature. The data are presented as mean values ± standard deviations (n = 3). Mean values with different letters are significantly different ($p < 0.05$).

3.2. HS-SPME/GC–MS analysis

HS-SPME/GC–MS was used to further study the effects of US and storage time on the volatile components of coconut water, and the results were shown in the Supplementary material. A total of 33 kinds of volatile compounds were detected, of which 32 kinds were identified. These volatile compounds include 6 kinds of alcohols, 6 kinds of esters, 4 kinds of aldehydes, 6 kinds of ketones, 7 kinds of alkanes, 1 kind of acid,

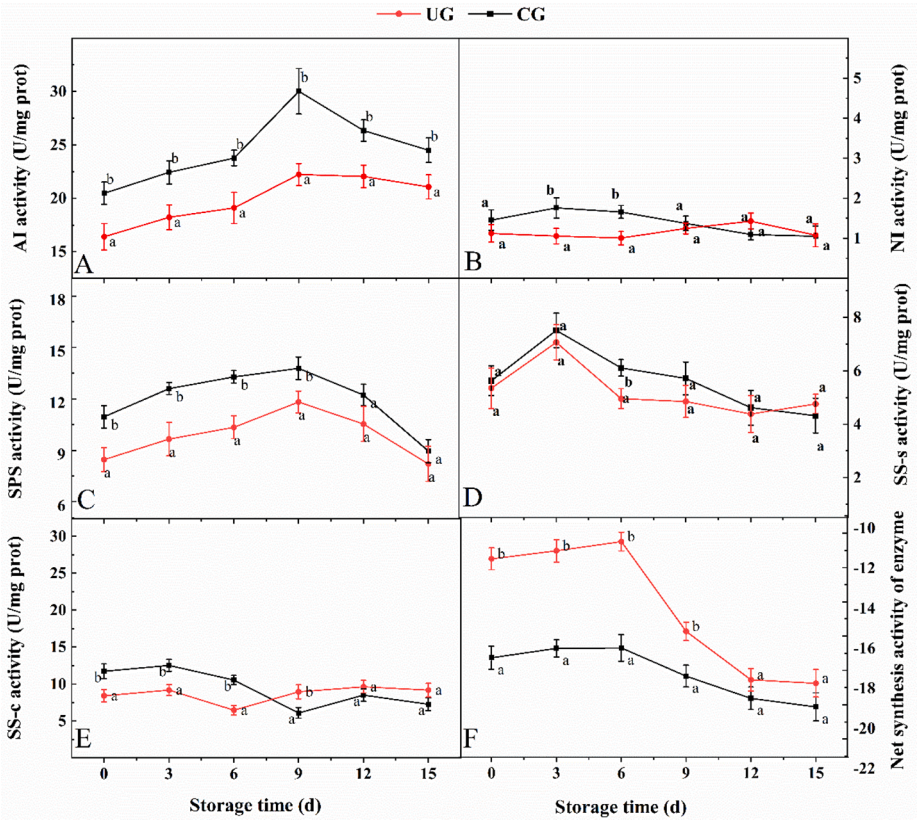

Fig. 5. Effect of US treatment on the activity of AI (A), NI (B), SPS (C), SS-s (D), SS-c (E) and net synthesis activity of enzyme (F) in coconut water stored at room temperature. Net synthesis activity of enzyme = (SS-s + SPS) − (AI + NI + SS-c). The data are presented as mean values ± standard deviations (n = 3). Mean values with different letters are significantly different ($p < 0.05$).

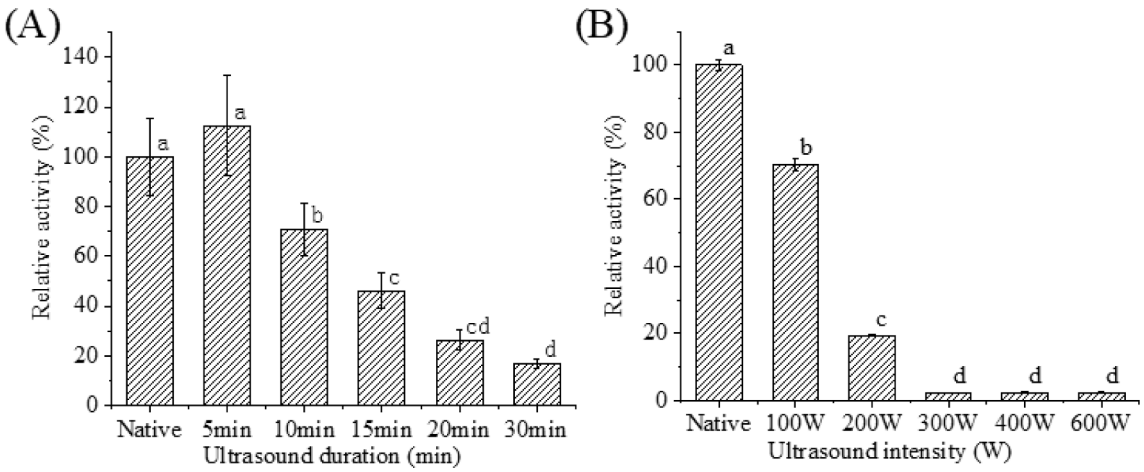

Fig. 6. Effect of US time (5–30 min, 200 W) (A) and intensity (100–600 W, 20 min) (B) on AI activity. The data are presented as mean values ± standard deviations (n = 3). Mean values with different letters are significantly different ($p < 0.05$).

2 kinds of phenols, etc.. The peak area percentage is used to measure the relative content of these volatile compounds in coconut water. There are 10 types of volatile compounds with a peak area percentage higher than one: linalool (31.62%), 2, 4-di-*tert*-butylphenol (23.13%), formic acid (13.71%), phenol, 2, 5-bis (1, 1-dimethylethyl)- (3.45%), phthalic acid, hept-4-yl isobutyl ester (2.94%), 1-octyn-3-ol, 4-ethyl- (2.71%), 2(3H)-furanone, 5-heptyldihydro- (1.38%), decanoic acid, methyl ester (1.16%), 2(3H)-furanone, 5-hexyldihydro- (1.15%) and alpha, -methy-, alpha, -[4-methyl-3-pentenyl] oxiranemethanol (1.01%). Linalool has the highest content and has strong green and sweet wooden-green scent, which can give coconut water a light and refreshing scent similar like alcohols. Meanwhile, furanone imparts the unique fruity flavor of coconut water [30,31].

Fig. 2 shows the heatmap of relative contents of volatile compounds in UG and CG at different storage time. The gradient color (-2 to 2) indicates the level of content, the darker red indicates the higher content, on the contrary, the darker blue indicates the lower content. In addition, the gradient color (0 to 14) indicates storage time, and the darker green stands for longer time. According to the changes in content with storage time, volatile compounds are divided into two groups. Decanal, dodecanal, 1-octyn-3-ol, 4-ethyl-, 2, 4-di-*tert*-butylphenol, 2(3H)-furanone, 5-heptyldihydro, formic acid and the not identified compound belong to the first group whose content gradually increases with storage time. The other left compounds are divided into the second group whose content gradually decreases with storage time. The increase of decanal and dodecanal contents may be attributed to the oxidative decomposition of lipids in coconut meat [32–34].

Fig. 3 shows the relative content of alcohols, esters, aldehydes, ketones, alkanes, acids and others in UG and CG at different storage time. There were no significant differences in the types and contents of volatile compounds between UG and CG. This may be due to the weak influence of US on the temperature of coconut water. The temperature of coconut water increased from 26.88 ± 0.82 °C to 31.56 ± 0.59 °C after US treatment, which was thought to be negligible for the changing of volatile compounds.

Alcohols have the highest content of volatile compounds, accounting for about 37%, which give coconut water a light and refreshing flavor. Prades et al. also proved that alcohols accounted for the highest proportion, up to 47.60% among the identified 36 volatile components in Thailand Aromatic Green Dwarf coconut water [35]. Moreover, as natural antioxidants, phenols accounts for about 26.60% of the total volatile components in coconut water. In addition, the content of formic acid is about 14% of the total volatile components, which gives coconut water a sweet and sour taste. However, the contents of esters, aldehydes and ketones are relatively low, but they are indispensable in terms of providing a complex fruity flavor.

3.3. Changes in the content of fructose, glucose and sucrose

The content of hexose (glucose and fructose) was significantly higher than that of sucrose in tender coconut water. The content of glucose and fructose accounted for 44.90% and 43.90% of the total sugar content, respectively, while the content of sucrose only accounted for about 1.02% [36]. As shown in Fig. 4, the contents of three sugars in UG were higher than that of CG during storage, and the change of sucrose content was most significant in these three sugars. The content of hexose manifested the same downward trend as sucrose throughout the storage period. In this study, it was supposed that the sweetness of sucrose was designated as 1.0, fructose was 1.5, and glucose was 0.7. After conversion, it was found that the sugar degree of UG was always higher than that of CG throughout the whole storage period. This may be due to the fact that US that combined with high pressure in the coconut body destroyed the structure of enzymes related to sucrose metabolism. Thus, the activity of enzymes was inhibited, resulting in relatively slow decrease in the content of glucose, fructose, and sucrose for UG [36].

3.4. Changes in enzyme activity related to sugar metabolism

As shown in Fig. 5, the activity of AI in coconut water was significantly higher than that of NI. The enhanced activity of AI can provide tissues hexose as the carbon source for the rapid growth, and there was a significant negative correlation between sucrose content and activity of AI. During the storage period, the activity of AI increased firstly and then decreased after 9 days, and the activity of AI in CG was always significantly higher than that of UG ($p < 0.05$). This may be attributed to the fact that the cavitation effect caused by high-intensity US under natural high-pressure environment of coconut destroyed the structure of the enzyme, resulting in inactivation of the enzyme [37].

However, the activity of AI was higher than that of SPS and SS, which indicates that AI is the key enzyme regulating sugar metabolism of coconut water. The activity of SPS showed a similar trend as AI, but there was no significant difference in the activity of SPS between UG and CG at the end of the storage period ($p > 0.05$). This indicates that the effect of SPS on sugar metabolism is not as significant as that of AI. As shown in Fig. 5D, the activity of SS-s showed an upward trend from 0 to 3 days and a downward trend from 3 to 15 days, and the difference between the UG and CG was not significant except the sixth day ($p > 0.05$). Unlike the trend of SS-s activity, the activity of SS-c decreased firstly and then increased (Fig. 5E), and the difference between UG and CG was not significant at the end of storage period (days 12–15) ($p > 0.05$). Finally,

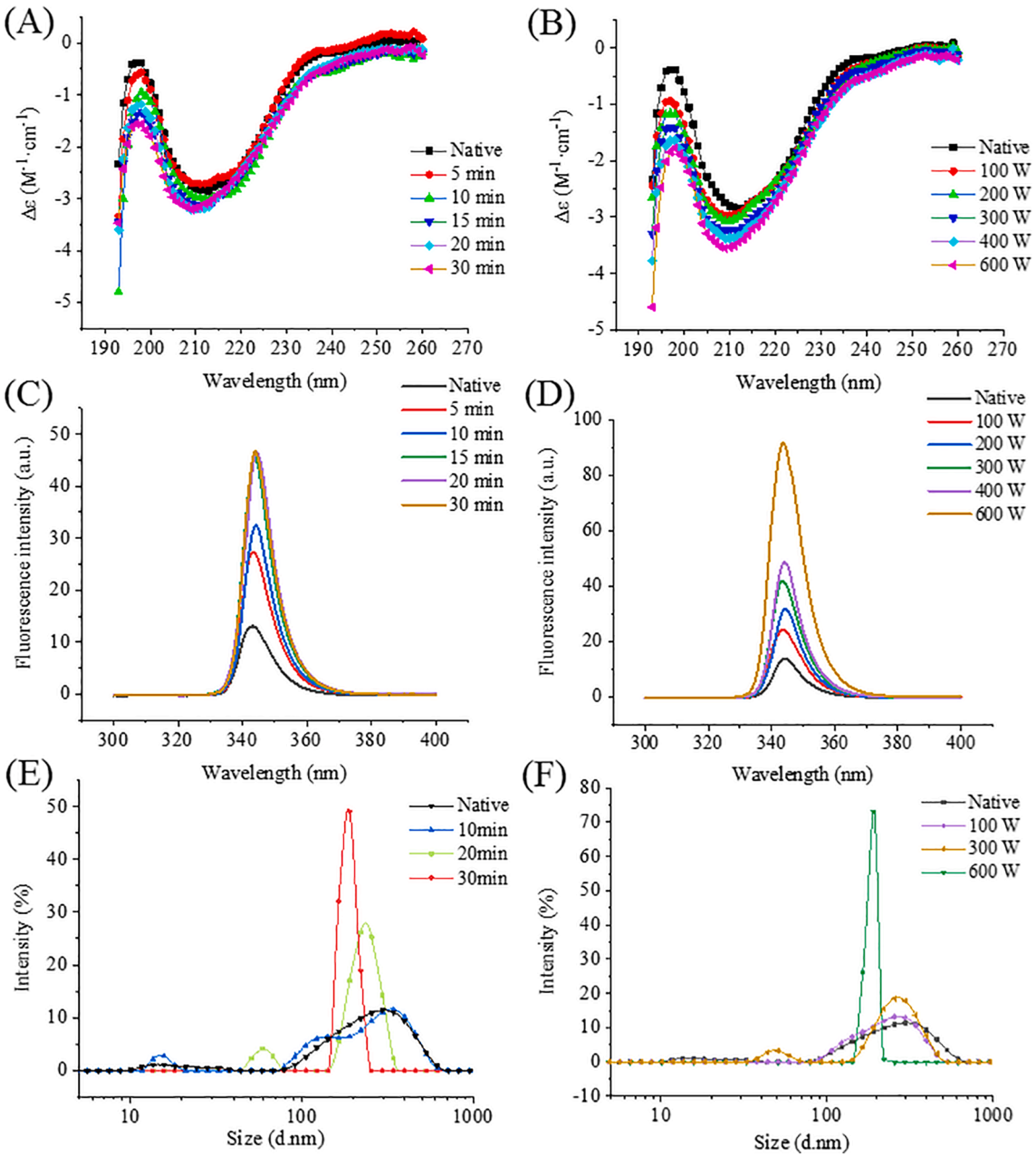

Fig. 7. CD (A, B), fluorescence spectra (C, D) and PSD pattern (E, F) of native and US-treated AI.

the net synthesis activity of sucrose metabolizing enzymes was calculated according to the following formula: the net synthesis activity of enzymes = (SS-s + SPS) - (AI + NI + SS-c). The net synthetic activity of enzymes was negative, and the value increased firstly and then decreased with the extension of storage time (Fig. 5F). This indicates that the activity of sucrose cleavage enzymes in coconut water is higher than that of sucrose synthase, and sucrose degradation plays a leading role during the storage process [38,39]. During the first 9 days of storage, the net synthesis activity of enzymes in UG was significantly higher than that of CG ($p < 0.05$), which was consistent with the dramatic decrease of sucrose content (Fig. 4C). All of the above results indicate that US treatment can increase the sucrose content during storage by inhibiting the activity of the enzymes related to sugar metabolism, especially AI.

3.5. Effect of US time and power on enzyme activity

Fig. 6A shows the activity of AI treated by US with different time at power of 200 W. The enzyme activity increased by 12% after 5 min of US treatment. As US time continued to increase, the enzyme activity gradually decreased, with significant differences between 10 min, 15 min, 20 min and 30 min, and the relative enzyme activity decreased to 71%, 41%, 36% and 18%, respectively. Short-time US cavitation may not destroy the structure of the enzyme or inactivate the enzyme. But it could increase contact opportunities and area between the substrate and the enzyme, an promote product molecules to leave the active center of the enzyme. However, with the prolongation of US time, the collapse of the bubbles caused by cavitation effect led to a sharp rise in temperature and pressure on the micro-scale, which may result in the inactivation of the enzymes [40].

As can be seen from Fig. 6B, the relative enzyme activity decreased significantly ($p < 0.05$) as US power increased. The activity of AI was

Table 1
Secondary structure contents of native and US-treated AI.

Samples	Secondary structure contents (%)			
	α-Helix	β-sheet	β-turn	Random coil
Native	12.37 ± 0.03c	40.78 ± 0.05a	15.23 ± 0.03a	31.63 ± 0.05e
100 W/20 min	12.25 ± 0.05b	41.14 ± 0.11b	15.24 ± 0.02a	31.36 ± 0.10d
200 W/20 min	12.15 ± 0.02a	41.42 ± 0.12c	15.23 ± 0.02a	31.16 ± 0.06c
300 W/20 min	12.13 ± 0.02a	41.82 ± 0.07d	15.24 ± 0.01a	30.84 ± 0.04b
400 W/20 min	12.14 ± 0.02a	41.81 ± 0.04d	15.24 ± 0.02a	30.74 ± 0.03ab
600 W/20 min	12.13 ± 0.02a	42.00 ± 0.12e	15.24 ± 0.02a	30.66 ± 0.02a
Native	12.37 ± 0.03d	40.78 ± 0.05a	15.23 ± 0.03a	31.63 ± 0.05d
200 W/5 min	12.34 ± 0.03c	41.12 ± 0.04b	15.24 ± 0.02a	31.26 ± 0.02c
200 W/10 min	12.24 ± 0.02b	41.26 ± 0.06c	15.26 ± 0.02a	31.19 ± 0.04b
200 W/15 min	12.24 ± 0.02b	41.44 ± 0.04d	15.24 ± 0.02a	31.10 ± 0.04a
200 W/20 min	12.22 ± 0.02b	41.49 ± 0.04de	15.27 ± 0.01a	31.08 ± 0.04a
200 W/30 min	12.12 ± 0.04a	41.54 ± 0.05e	15.26 ± 0.02a	31.08 ± 0.03a

The data are presented as mean values ± standard deviations (n = 3). Mean values with different letters in each column are significantly different ($p < 0.05$).

reduced by 30% under US treatment at 100 W, after which the activity was reduced to 19.30% under US treatment at 200 W. In particular, when US power exceeded 300 W, AI was almost completely inactivated. To sum up, both high-power short-time and low-power long-time US can efficiently inhibit the activity of enzymes, and the former has stronger effect on enzyme inactivation. High-intensity US treatment provided more energy on the active center of AI, causing the explosion of hydrophilic group of the active center, thus promoting a more polar environment for the active center. When the hydrophobic microenvironment was destroyed, the catalytic activity of AI would be inhibited. Therefore, increased US treatments (extended duration and intensity) caused more shear forces and sonolysis, leading to more decrease in AI activity [20].

3.6. CD, fluorescence spectra and PSD analysis

The structural integrity of enzyme molecule is essential for its catalytic function. In order to study the effect of US treatment on molecular structure of AI, CD, fluorescence spectra and PSD pattern were further investigated. CD is an effective technique to study secondary structure of protein. The secondary structure of protein includes α-helix, β-sheet, β-turn and random coils. CD spectrum of α-helix is characterized by two negative peaks at 208 and 222 nm along with a positive peak at 192 nm. The characteristic peaks of β-sheet contain a negative peak at 217 nm and a positive peak at 195 nm. And β-turn typically consists of a positive peak at 207.5 or 209 nm and a negative peak near 227 nm. Meanwhile, random coils are characterized by a single peak below 200 nm [41,42]. CD spectra of US-treated AI at different time and power are shown in Fig. 7A and B. The results showed that a positive peak appeared at 197 nm and a negative peak appeared at 210 nm, which are typical characteristic peaks of β-sheet. The detailed secondary structure information is shown in Table 1. The content of α-helix, β-sheet, β-turn and random coils of native AI were 12.37%, 40.78%, 15.23% and 31.63%, respectively, which indicates that β-sheets and random coils are the main forms in the secondary structure of native AI. With the increase of US time and power, the content of α-helix and random coils decreased, while the content of β-sheet increased. Secondary structure of protein depends not only on the composition and arrangement of amino acids, but also on the non-bonding interactions between peptide chains, such as hydrogen bonds, van der Waals forces, hydrophobic interactions, electrostatic interactions, etc.. US treatment can destroy these non-covalent bonds, leading to destruction of natural secondary structure of protein, thereby

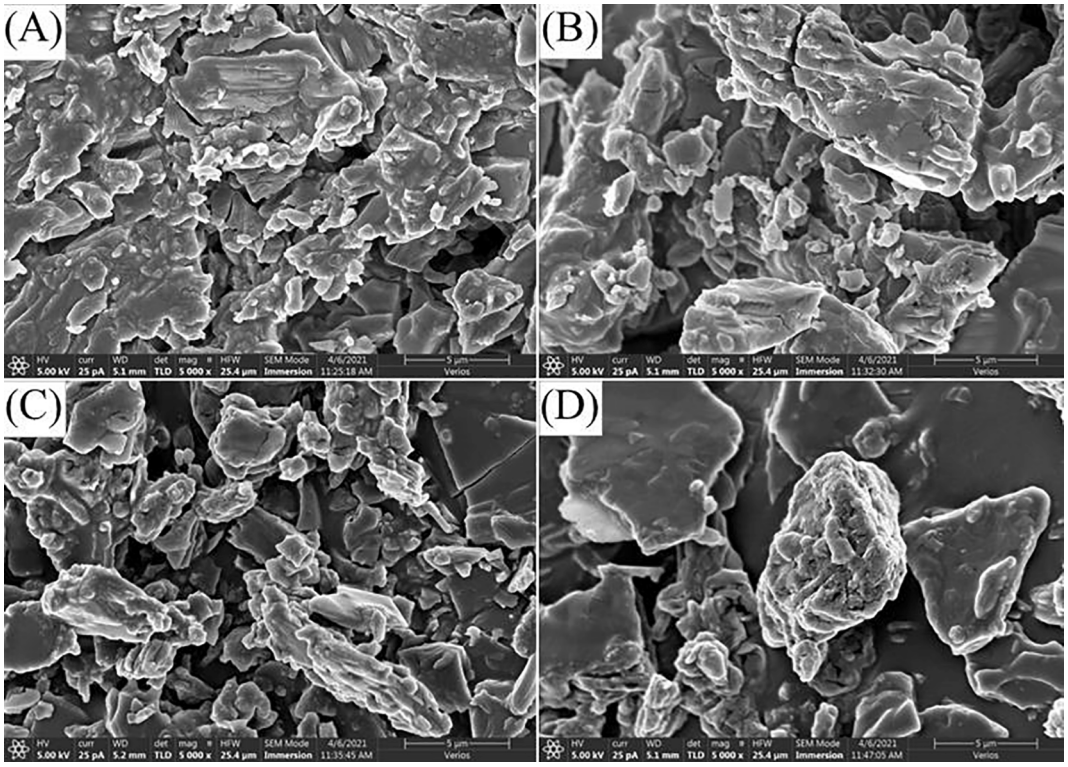

Fig. 8. SEM images of native (A) and US-treated AI with different powers, including 100 W (B), 300 W (C) and 600 W (D).

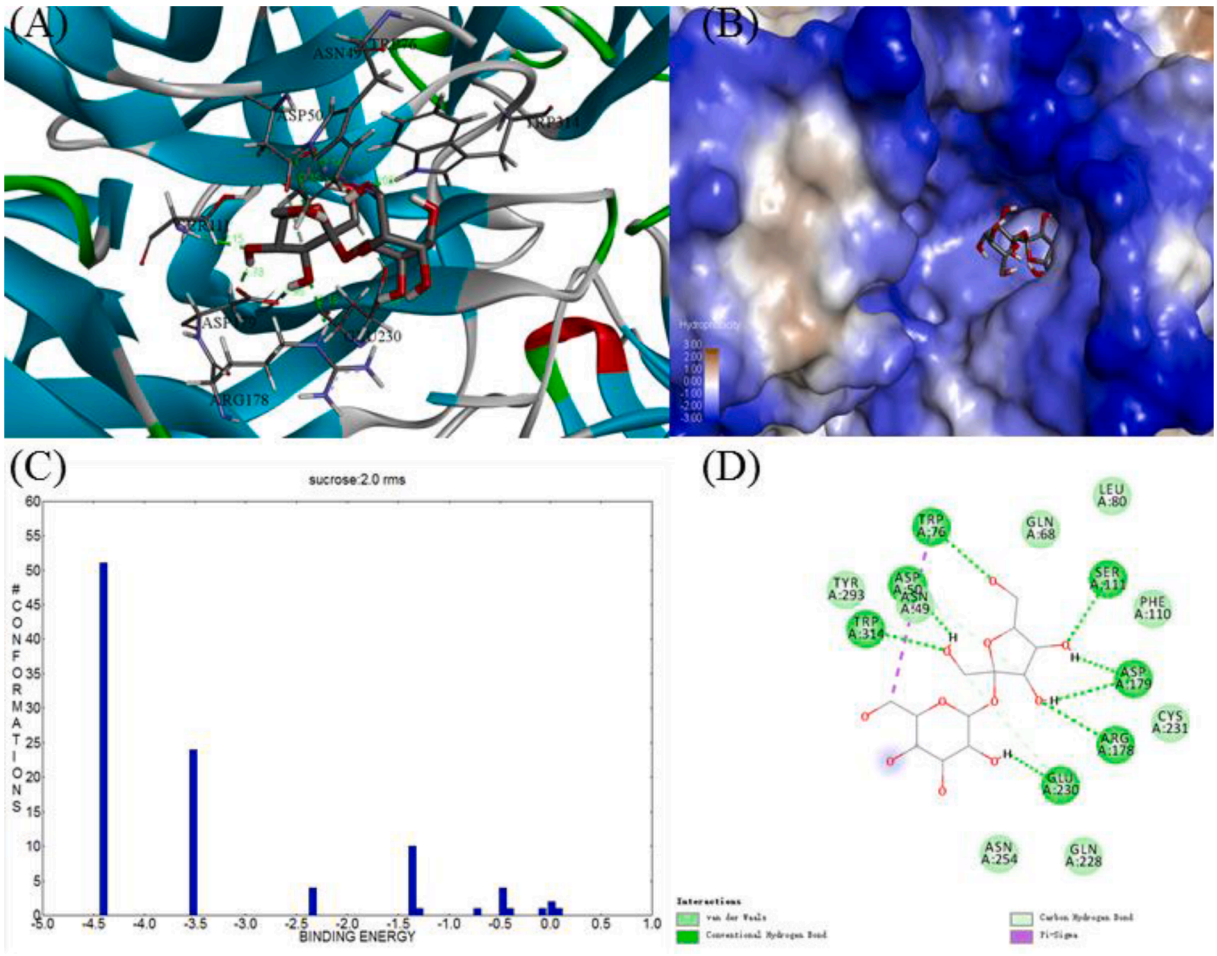

Fig. 9. Molecular docking results of sucrose with AI molecule.

causing the loss of original physiological function [14–16]. Gülseren et al. showed that US treatment increased the content of α-helix of albumin, and decreased the content of β-sheet and β-turn, resulting in increased hydrophobicity of the surface of albumin, and the damage to secondary structure of protein by US treatment was irreversible [43].

Fluorescence spectroscopy is a useful technique for studying tertiary structural transformations in proteins. Intrinsic fluorescence of aromatic amino acid residues (Trp, Tyr and Phe, especially Trp) is extremely sensitive to the polarity of microenvironment [44]. When the polarity of the hydrophobic microenvironment of AI molecule changes, the fluorescence intensity and the maximum emission wavelength (λmax) of Trp residues will also be changed. As shown in Fig. 7C and D, the λmax of native AI was 343.2 nm with an intensity of 13.023 a.u.. With the increase of time and power of US treatment, λmax had a blue shift, which indicates that US treatment caused Trp residues to be buried in the interior of AI molecule. A similar result was also confirmed by the change in fluorescence intensity of polyphenol oxidase by US treatment (200 W, 30 min) [20]. In addition, as the power and time of US increased, the fluorescence intensity of AI gradually increased, which indicates that Trp residues are placed in a more hydrophobic microenvironment. This may be attributed to the fact that some Trp residues may have been associated within non-polar region because of polymerization, aggregation or peptide-peptide association [45]. This conformational transformation of tertiary structure of enzyme molecule is unfavorable for the combination of substrate and the active cavity. Therefore, as the US intensity increases, the activity of AI becomes lower and lower.

PSD patterns for UG and CG are shown in Fig. 7E and F. Native AI showed two sections of PSD pattern, one peak at 15.7 nm with the volume fraction of 6.40%, and another peak at 295.3 nm with the highest volume fraction (11.40 %). The effect of US time on the PSD pattern of AI is shown in Fig. 7E. The results showed that AI particles with small particle size tended to aggregate, while AI particles with large particle size dissociated at 20 to 30 min and reached the highest volume fraction (49%) at 30 min with a peak size of 190.1 nm. The effect of US power on the PSD pattern of AI is shown in Fig. 7F. In general, as US intensity increased, the small AI particles aggregated and the large AI particles separated. The maximum peak diameter (190.1 nm) with the highest volume fraction (73.20%) was achieved after US treatment at 600 W. This was attributed to the fact that US treatment produced a large number of tiny bubbles in the medium, which will implode and generate huge shear forces. The shear force could break the intermolecular and intramolecular connections, thus leads to the aggregation of AI molecule as well as the fragmentation of these aggregates [46]. Therefore, US treatment can lead to homogenization of AI molecule by disrupting protein–protein interactions.

3.7. SEM analysis

The microstructure of native and US-treated AI at different powers was observed by SEM (Fig. 8). Native AI with small and large particle sizes were closely distributed but not interconnected (Fig. 8A). After US treatment with power of 100 W and 300 W, AI molecule with small particle size tended to aggregate, while AI molecule with large particle size dissociated (Fig. 8B and C). With the increase of US power, the particle size of AI molecule became more uniform (Fig. 8D), which was consistent with the result of PSD pattern.

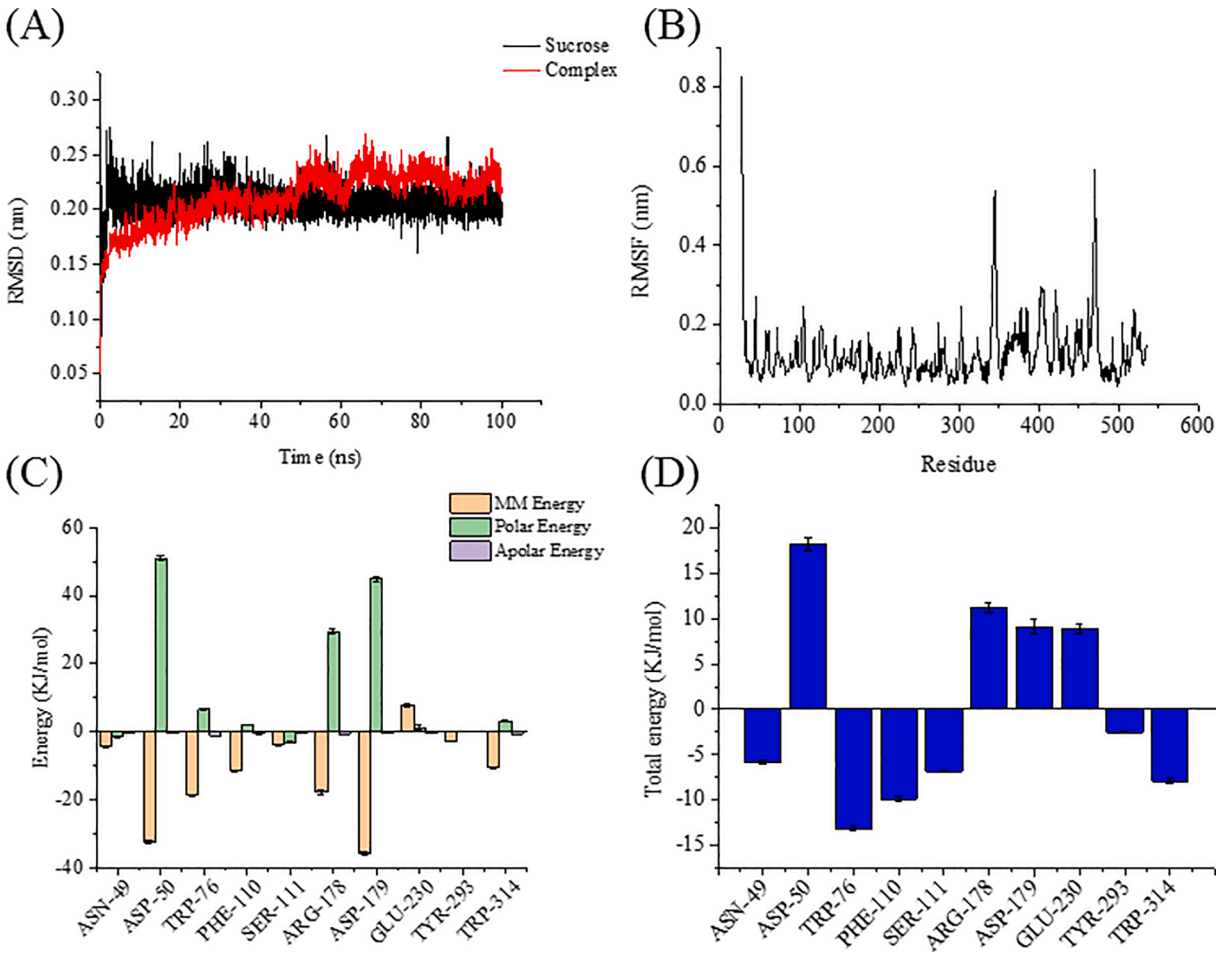

Fig. 10. RMSD, RMSF, and the contribution of key amino acids to the total binding free energy and energy decomposition analysis of AI/sucrose complex.

3.8. Molecular docking and molecular dynamics analysis

Molecular docking and molecular dynamics are very effective tools to study the interaction between small molecule ligands and macromolecular receptors. Fig. 9C shows the cluster analysis with tolerance (RMS tolerance value) of 2.0. The 100 configurations were ranked by binding energy, and the cluster with the lowest binding energy (−4.4 kcal/mol) contained 51 configurations. The conformations with the lowest binding energy were taken as the research objects for further analysis. Fig. 9B shows the binding site of sucrose to AI molecule. The gradient color (-3 to 3) indicates the degree of hydrophobicity. The darker brown indicates the stronger the hydrophobicity, on the contrary, the darker blue indicates the weaker hydrophobicity. As we can see from the picture, sucrose molecule can enter the hydrophobic active cavity of AI molecule and interact with key amino acids.

The interactions of sucrose with key amino acids of AI molecule are shown in Fig. 9A (3D diagram) and Fig. 9D (2D diagram). The number on dotted line indicates the distance between hydroxyl group and amino acid (Fig. 9A). The smaller the distance is, the stronger the hydrogen bond is. Two conventional hydrogen bonds were formed between hydroxyl group at Fructofuranose-C-1-position of sucrose molecule and key amino acids, including ASP A: 50 and TRP A: 341. Meanwhile, a weaker carbon hydrogen bond was formed between Fructofuranose-C-1-position of sucrose molecule and key amino acid GLU A: 230. Moreover, two conventional hydrogen bonds were formed between hydroxyl group at Fructofuranose-C-3-position of sucrose molecule and key amino acids ARG A: 178 and ASP A: 179. Besides, a weaker carbon hydrogen bond was formed between Fructofuranose-C-3-position of sucrose molecule and key amino acid ASP A: 50. Two conventional hydrogen bonds were formed between hydroxyl group at Fructofuranose-C-4-position of sucrose molecule and key amino acids SER A: 111 and ASP A: 179. In addition, a conventional hydrogen bond was formed between hydroxyl group at Fructofuranose-C-6-position of sucrose molecule and key amino acid TRP A: 76. A conventional hydrogen bond was formed between hydroxyl group at Glucopyranose-C-2-position of sucrose molecule and key amino acid GLU A: 230. Besides, a hydrophobic interaction (Pi-Sigma hyperconjugation) was formed between carbon hydrogen bond at Glucopyranose-C-6-position of sucrose molecule and the benzene ring of key amino acid TRP A: 76. These amino acids in the active cavity of AI molecule are of great significance to the recognition and binding of the substrate sucrose molecule [47].

Root mean square deviation (RMSD) and root mean square fluctuation (RMSF) of AI/sucrose complex are shown in Fig. 10, which can measure structural changes of the complex. As can be seen from Fig. 10A, RMSD value of sucrose molecule had a mutation at 1.5 ns, after which it reached an equilibrium state. This indicates that the structure of sucrose molecule is adjusted to the suitable state that will combine with key amino acids in the active cavity of AI molecule. However, the structure of AI/sucrose complex reached an equilibrium state after 50 ns, with the fluctuation of RMSD was <0.1 nm. This means that the structure of sucrose and AI molecule had been adjusted to the most stable state after mutation.

Fig. 10B shows the RMSF values of amino acids in AI skeleton. It can be seen that amino acids with higher RMSF values are LYS-45, ASP-105, ILE-129, TYR-225, LYS-385 and PRO-406, and these amino acids are all located in random coils. In addition, ASP-187, ASN-241, PHE-274, HIS-303, GLU-345, LYS-377, ASN-421, ASP-471, GLU-505 and GLU-519 are located in β-turn and also have larger RMSF values. This may be

Table 2
Binding free energy of AI/sucrose complex.

Energy terms (KJ/mol)	AI/sucrose complex
VDW Energy	−153.484 ± 13.459
EE Energy	−185.479 ± 12.697
Polar Energy	257.688 ± 14.383
Apolar Energy	−14.887 ± 0.461
Delta Total	−96.164 ± 11.604

The data are presented as mean values ± standard deviations (n = 3). VDW Energy: van der Waals energy; EE Energy: Electrostatic energy; Polar Energy: Polar solvation energy; Apolar Energy: Non-polar solvation energy; Delta Total: Total binding free energy.

attributed to the fact that amino acids located in β-turn and random coils have more flexible conformations that can adjust structures of AI molecule in time to combine with sucrose. In contrast, ASN-49, ASP-50, TRP-76, PHE-110, SER-111, ARG-178, ASP-179, GLU-230, TYR-293 and TRP-314 are located in the active cavity of AI molecule and have smaller RMSF values due to the strong binding of these amino acids to sucrose molecule [48].

In order to investigate the stability of AI/sucrose complex, MM/PBSA method was used to calculate the binding free energy. As we can see from Table 2, the total binding free energy of AI/sucrose complex was −96.164 KJ/mol. Besides, van der Waals energy, electrostatic energy and non-polar solvation energy were −153.484 KJ/mol, −185.479 KJ/mol and −14.887 KJ/mol, respectively, which were beneficial to the combination of AI and sucrose molecules. However, the polar solvation energy was 257.688 KJ/mol, which was detrimental to the combination of AI and sucrose molecules. The contribution of key amino acids to the total binding free energy and energy decomposition are shown in Fig. 10C. Except for GLU-230, MM energy of key amino acid of AI/sucrose complex is all negative, which may be conducive to generation of hydrogen bonds. The total binding free energy of AI/sucrose complex was further analyzed in Fig. 10D. The total binding energy of ASP-50, ARG-178, ASP-179 and GLU-230 are positive, which is unfavorable for the complex due to the greater polarity of these amino acids. On the contrary, the total binding energy of ASN-49, TRP-76, PHE-110, SER-111, TYR-293 and TRP-314 are negative and play a positive role in the binding of AI and sucrose molecules [49]. Results from molecular dynamic analysis indicate that hydrophobic amino acids in the active cavity of AI are crucial for the recognition and binding of the substrate sucrose molecule. However, high-intensity US treatment destroyed the natural conformation of AI molecule, and fluorescence spectra showed that these hydrophobic amino acids were encapsulated, which was unfavorable for the recognition and binding of substrate. Therefore, high-intensity US treatment prevented the recognition and binding of sucrose and AI molecules, thereby inhibiting the decomposition of sucrose.

4. Conclusion

In this study, US treated coconut water had a higher content of TSS and sugar/acid ratio along with a lower pH value and conductivity, thus had a higher sweetness. There was no significant difference in the content of volatile compounds between UG and CG. US treatment caused inactivation of four kinds of enzymes related to sugar metabolism, especially AI. Structural characterization showed that the secondary and tertiary structure of AI molecule was destroyed by US. Molecular docking and molecular dynamics showed that US treatment prevented the recognition and binding of sucrose and AI molecules, thereby inhibiting the decomposition of sucrose. In conclusion, our results indicate that US can inhibit the activity of AI and maintain the sugar content to increase the quality as well as extend the shelflife of coconut water, which will bring more commercial value.

CRediT authorship contribution statement

Jilin Wu: Writing – original draft, Methodology, Software. **Haiming Chen:** Methodology. **Wenxue Chen:** Data curation, Resources. **Qiuping Zhong:** Methodology. **Ming Zhang:** Writing – review & editing, Data curation. **Weijun Chen:** Methodology.

Declaration of Competing Interest

The authors declare that they have no known competing financial interests or personal relationships that could have appeared to influence the work reported in this paper.

Acknowledgements

This research was supported by the High-level Talent Project of Hainan Natural Science Foundation (2019RC128).

Appendix A. Supplementary data

Supplementary data to this article can be found online at https://doi.org/10.1016/j.ultsonch.2021.105780.

References

[1] A. Prades, M. Dornier, N. Diop, J.P. Pain, Coconut water preservation and processing: a review, Fruits 67 (2012) 157–171.
[2] Y. Zhang, W. Chen, H. Chen, Q. Zhong, Y. Yun, W. Chen, Metabolomics analysis of the deterioration mechanism and storage time limit of tender coconut water during storage, Foods 9 (2020) 1–18.
[3] D. Campbell-Falck, T. Thomas, T.M. Falck, N. Tutuo, K. Clem, The intravenous use of coconut water, Am. J. Emerg. Med. 18 (2000) 108–111.
[4] A. Prades, M. Dornier, N. Diop, J.P. Pain, Coconut water uses, composition and properties: a review, Fruits 67 (2012) 87–107.
[5] M. Kumar, S.S. Saini, P.K. Agrawal, P. Roy, D. Sircar, Nutritional and metabolomics characterization of the coconut water at different nut developmental stages, J. Food Compos. Anal. 96 (2021), 103738.
[6] B. Nguyen-Quoc, C.H. Foyer, A role for 'futile cycles' involving invertase and sucrose synthase in sucrose metabolism of tomato fruit, J. Exp. Bot. 52 (2001) 881–889.
[7] Y. Chen, Y. Ge, J. Zhao, M. Wei, C. Li, J. Hou, Y. Cheng, J. Chen, Postharvest sodium nitroprusside treatment maintains storage quality of apple fruit by regulating sucrose metabolism, Postharvest Biol. Technol. 154 (2019) 115–120.
[8] L. Yang, J. Chen, X. Sun, J. Li, N. Chen, Inhibition of sucrose and galactosyl-sucrose oligosaccharide metabolism in leaves and fruits of melon (Cucumis melo L.) under low light stress, Sci. Hortic. 244 (2019) 343–351.
[9] A.R. Fernie, L. Willmitzer, R.N. Trethewey, Sucrose to starch: a transition in molecular plant physiology, Trends Plant Sci. 7 (2002) 35–41.
[10] Q. Jiang, M. Zhang, B. Xu, Application of ultrasonic technology in postharvested fruits and vegetables storage: a review, Ultrason. Sonochem. 69 (2020), 105261.
[11] S.Ş. Ercan, Ç. Soysal, Effect of ultrasound and temperature on tomato peroxidase, Ultrason. Sonochem. 18 (2011) 689–695.
[12] M.M. Delgado-Povedano, M.L. De Castro, A review on enzyme and ultrasound: A controversial but fruitful relationship, Anal. Chim. Acta 889 (2015) 1–21.
[13] Z.M. Tian, M.X. Wan, S.P. Wang, J.Q. Kang, Effects of ultrasound and additives on the function and structure of trypsin, Ultrason. Sonochem. 11 (2004) 399–404.
[14] Z.V. Rachinskaya, E. Karasyova, D. Metelitza, Inactivation of glucose-6-phosphate dehydrogenase in solution by low-and high-frequency ultrasound, Appl. Biochem. Microbiol. 40 (2004) 120–128.
[15] C. Basto, C.J. Silva, G. Gübitz, A. Cavaco-Paulo, Stability and decolourization ability of Trametes villosa laccase in liquid ultrasonic fields, Ultrason. Sonochem. 14 (2007) 355–362.
[16] Z.L. Yu, W.C. Zeng, X.L. Lu, Influence of ultrasound to the activity of tyrosinase, Ultrason. Sonochem. 20 (2013) 805–809.
[17] N.S. Terefe, R. Buckow, C. Versteeg, Quality-related enzymes in plant-based products: effects of novel food-processing technologies part 3: ultrasonic processing, Crit. Rev. Food Sci. Nutr. 55 (2015) 147–158.
[18] L.H. Thompson, L. Doraiswamy, Sonochemistry: science and engineering, Ind. Eng. Chem. Res. 38 (1999) 1215–1249.
[19] T.M. Qureshi, M. Nadeem, F. Maken, A. Tayyaba, H. Majeed, M. Munir, Influence of ultrasound on the functional characteristics of indigenous varieties of mango (Mangifera indica L.), Ultrason. Sonochem. 64 (2020), 104987.
[20] A. Iqbal, A. Murtaza, K. Marszałek, M.A. Iqbal, M.F. Chughtai, W. Hu, F.J. Barba, J. Bi, X. Liu, X. Xu, Inactivation and structural changes of polyphenol oxidase in quince (Cydonia oblonga Miller) juice subjected to ultrasonic treatment, J. Sci. Food Agric. 100 (2020) 2065–2073.
[21] N. Huang, X. Cheng, W. Hu, S. Pan, Inactivation, aggregation, secondary and tertiary structural changes of germin-like protein in Satsuma mandarine with high

polyphenol oxidase activity induced by ultrasonic processing, Biophys. Chem. 197 (2015) 18–24.
[22] L. Zhou, W. Liu, L. Zou, Z. Xiong, X. Hu, J. Chen, Aggregation and conformational change of mushroom (Agaricus bisporus) polyphenoloxidase subjected to thermal treatment, Food Chem. 214 (2017) 423–431.
[23] Q. Liu, R. Geng, J. Zhao, Q. Chen, B. Kong, Structural and gel textural properties of soy protein isolate when subjected to extreme acid pH-shifting and mild heating processes, J. Agric. Food Chem. 63 (2015) 4853–4861.
[24] G.M. Morris, R. Huey, W. Lindstrom, M.F. Sanner, R.K. Belew, D.S. Goodsell, A. J. Olson, AutoDock4 and AutoDockTools4: Automated docking with selective receptor flexibility, J. Comput. Chem. 30 (2009) 2785–2791.
[25] M.J. Latallo, G.A. Cortina, S. Faham, R.K. Nakamoto, P.M. Kasson, Predicting allosteric mutants that increase activity of a major antibiotic resistance enzyme, Chem. Sci. 8 (2017) 6484–6492.
[26] J. Ren, X. Yuan, J. Li, S. Lin, B. Yang, C. Chen, J. Zhao, W. Zheng, H. Liao, Z. Yang, Assessing the performance of the g_mmpbsa tools to simulate the inhibition of oseltamivir to influenza virus neuraminidase by molecular mechanics Poisson-Boltzmann surface area methods, J. Chin. Chem. Soc. 67 (2020) 46–53.
[27] F. Famiani, N.G. Cultrera, A. Battistelli, V. Casulli, P. Proietti, A. Standardi, Z. H. Chen, R.C. Leegood, R.P. Walker, Phosphoenolpyruvate carboxykinase and its potential role in the catabolism of organic acids in the flesh of soft fruit during ripening, J. Exp. Bot. 56 (2005) 2959–2969.
[28] K. Meethaworn, J. Siriphanich, Postharvest behavior during storage of young coconut (Cocos nucifera L.) at different temperatures, Acta Hort. 1091 (2015) 125–131.
[29] C. Wei, J. Qiao, X. Tang, Q. Yan, L. Tang, Z. Ma, Effect of Bagging on the Content of Sugar and Acid in Postharvest "Jinhuang", Mango Fruit, E3S Web of Conf. 145 (2020) 01032.
[30] A.M.d. Fonseca, A. Bizerra, J.S.N.d. Souza, F.J.Q. Monte, M.d.C.F.d. Oliveira, M.C. d. Mattos, G.A. Cordell, R. Braz-Filho, T.L. Lemos, Constituents and antioxidant activity of two varieties of coconut water (Cocos nucifera L.), Rev. Bras. Farmacogn. 19 (2009) 193–198.
[31] V. Luckanatinvong, S. Mahatheeranont, J. Siriphanich, Variation in the aromatic nature of Nam-Hom coconut depends on the presence and contents of 2-acetyl-1-pyrroline, Sci. Hortic. 233 (2018) 277–282.
[32] K. Meethaworn, J. Siriphanich, Volatiles and enzymes involved in off-flavor development in trimmed young coconut water during low temperature storage, Acta Hortic. 1178 (2017) 105–110.
[33] F. De Marchi, E. Aprea, I. Endrizzi, M. Charles, E. Betta, M.L. Corollaro, M. Cappelletti, G. Ferrentino, S. Spilimbergo, F. Gasperi, Effects of pasteurization on volatile compounds and sensory properties of coconut (Cocos nucifera L.) water: thermal vs. high-pressure carbon dioxide pasteurization, Food Bioprocess Technol. 8 (2015) 1393–1404.
[34] M.D. Purkayastha, D. Kalita, V.K. Das, C.L. Mahanta, A.J. Thakur, M.K. Chaudhuri, Effects of L-ascorbic acid addition on micro-filtered coconut water: preliminary quality prediction study using 1H-NMR, FTIR and GC-MS, Innov. Food Sci. Emerg. Technol. 13 (2012) 184–199.
[35] A. Prades, R.R.A. Assa, M. Dornier, J.P. Pain, R. Boulanger, Characterisation of the volatile profile of coconut water from five varieties using an optimised HS-SPME-GC analysis, J. Sci. Food Agric. 92 (2012) 2471–2478.
[36] U. Santoso, K. Kubo, T. Ota, T. Tadokoro, A. Maekawa, Nutrient composition of kopyor coconuts (Cocos nucifera L.), Food Chem. 57 (1996) 299–304.
[37] G. Huang, S. Chen, C. Dai, L. Sun, W. Sun, Y. Tang, F. Xiong, R. He, H. Ma, Effects of ultrasound on microbial growth and enzyme activity, Ultrason. Sonochem. 37 (2017) 144–149.
[38] X. Shao, Y. Zhu, S. Cao, H. Wang, Y. Song, Soluble sugar content and metabolism as related to the heat-induced chilling tolerance of loquat fruit during cold storage, Food Bioprocess Technol. 6 (2013) 3490–3498.
[39] Y. Wei, F. Xu, X. Shao, Changes in soluble sugar metabolism in loquat fruit during different cold storage, Int. J. Food Sci. Technol. 54 (2017) 1043–1051.
[40] S. Liu, Y. Liu, X. Huang, W. Yang, W. Hu, S. Pan, Effect of ultrasonic processing on the changes in activity, aggregation and the secondary and tertiary structure of polyphenol oxidase in oriental sweet melon (Cucumis melo var. makuwa Makino), J. Sci. Food Agric. 97 (2017) 1326–1334.
[41] C. Drapaneni, P. Ghosh, T. Ghosh, G. Maayan, Unique β-turn peptoid structures and their application as asymmetric catalysts, Chem. Eur. J. 26 (2020) 9573–9579.
[42] H. Zarei, A. Aramvash, M.S. Seyedkarimi, Investigating the stability of RADA16 peptide nanofibers using CD spectra, Int. J. Pept. Res. Ther. 25 (2019) 265–272.
[43] İ. Gülseren, D. Güzey, B.D. Bruce, J. Weiss, Structural and functional changes in ultrasonicated bovine serum albumin solutions, Ultrason. Sonochem. 14 (2007) 173–183.
[44] M.I. Viseu, T.I. Carvalho, S.M. Costa, Conformational transitions in β-lactoglobulin induced by cationic amphiphiles: equilibrium studies, Biophys. J . 86 (2004) 2392–2402.
[45] C. Tang, X.Q. Yang, Z. Chen, H. Wu, Z.Y. Peng, Physicochemical and structural characteristics of sodium caseinate biopolymers induced by microbial transglutaminase, J. Food Biochem. 29 (2005) 402–421.
[46] J. Chandrapala, B. Zisu, M. Palmer, S. Kentish, M. Ashokkumar, Effects of ultrasound on the thermal and structural characteristics of proteins in reconstituted whey protein concentrate, Ultrason. Sonochem. 18 (2011) 951–957.
[47] M. Sakakibara, D. Wang, R. Takahashi, K. Takahashi, S. Mori, Influence of ultrasound irradiation on hydrolysis of sucrose catalyzed by invertase, Enzyme Microb. Technol. 18 (1996) 444–448.
[48] Y. Wang, Q.C. Zheng, J.L. Zhang, Y.L. Cui, Q. Xue, H.X. Zhang, Highlighting a π-π interaction: a protein modeling and molecular dynamics simulation study on Anopheles gambiae glutathione S-transferase 1–2, J. Mol. Model. 19 (2013) 5213–5223.
[49] D.R. Sun, Q.C. Zheng, H.X. Zhang, Probing the interaction mechanism of small molecule inhibitors with matriptase based on molecular dynamics simulation and free energy calculations, J. Biomol. Struct. Dyn. 35 (2017) 755–764.